

# Injectable Double-Network Hydrogel-Based Three-Dimensional Cell Culture Systems for Regenerating Dental Pulp

Bing Han,<sup>†</sup> Chunling Cao,<sup>†</sup> Aijing Wang, Yanran Zhao, Moran Jin, Yuhan Wang, Shuqin Chen, Min Yu, Zhenzhong Yang,\* Xiaozhong Qu,\* and Xiaoyan Wang\*



Cite This: *ACS Appl. Mater. Interfaces* 2023, 15, 7821–7832



Read Online

ACCESS |



Metrics & More



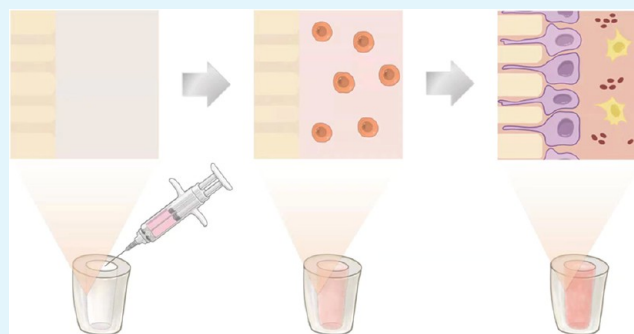
Article Recommendations



Supporting Information

**ABSTRACT:** The regeneration of dental pulp tissue is very important, but difficult, in dentistry. The biocompatibility, water content, and viscoelastic properties of pulp-like tissue must be optimized to achieve the efficient transfer of metabolites and nutrients, a suitable degradation rate, distribution of encapsulated cells, injectability, and gelation *in situ* under physiological conditions. As promising materials for pulp regeneration, hydrogel scaffolds have been produced to simulate the extracellular matrix and transmit signaling molecules. It is imperative to develop hydrogels to effectively regenerate pulp tissue for clinical application. Here, two injectable double-network (DN) hydrogel-based three-dimensional (3D) cell culture systems were developed for regenerating dental pulp. The microstructure, mechanical property, rheology property, and degradation behavior of the injectable DN glycol chitosan-based hydrogels in a simulated root canal model were characterized and compared to a single-network (SN) glycol chitosan-based hydrogel. Human dental pulp stem cells (hDPSCs) were then encapsulated into the GC-based hydrogels for the regeneration of pulp tissue, and the biological performance was investigated both *in vitro* and *in vivo*. The results showed that the DN hydrogels had ideal injectability under physiological conditions due to the dynamic nature of the crosslinks. Besides, the DN hydrogels exhibited better mechanical properties and longer degradation duration than the corresponding SN hydrogel. As a 3D cell culture system, the characteristics of the DN hydrogel facilitated odontogenic differentiation and mineralization of hDPSCs *in vitro*. Further *in vivo* analysis confirmed that the chemical composition, matrix stiffness, and degradation rate of the DN hydrogel matched those of pulp-like fibrous connective tissue, which might be related to Smad3 activation. These findings demonstrate that DN glycol chitosan-based hydrogels are suitable for the regeneration of pulp tissue.

**KEYWORDS:** pulp regeneration, injectable hydrogel, double network, human dental pulp stem cells, matrix stiffness



## 1. INTRODUCTION

Good oral health, including the teeth, is particularly important to overall health. Besides mastication, the teeth play important roles in speech, breathing, maintaining a patent airway, and serving as a foundation for the vertical dimensions of the face. Histologically, the teeth are composed of four different types of material: enamel, which covers the crown of the tooth and is the hardest substance in the body; dentin, a hard calcareous material that constitutes the principal mass of the tooth; pulp, which contains the nerves and blood vessels that supply the tooth; and cementum, a mineralized tissue covering the root of the tooth that sits inside the gum socket. The most peripheral layer of the dental pulp is composed of connective tissue that is rich in blood vessels and a layer of odontoblasts that secretes the dentin matrix. Loss of the enamel and dentin is mainly due to the formation of dental caries. Hence, timely treatment of dental caries is important to prevent pulpitis and periapical periodontitis. In root canal therapy, the infected pulp is removed and the root canals are cleaned, shaped, and filled

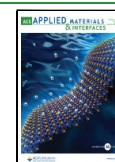
with gutta-percha materials to prevent recontamination. However, after root canal therapy, the tooth becomes brittle and is prone to fracture due to the lack of pulp tissue, resulting in tooth loss.<sup>1,2</sup> Hence, maintaining the pulp tissue is very important for oral health.

Continued progress in biomaterials research has facilitated reconstruction of impaired tissues and organs, including cartilage and skin.<sup>3,4</sup> The goal of regenerative endodontics is to promote recovery of normal pulp function in inflamed and necrotic teeth.<sup>5,6</sup> However, optimization of a scaffolding system for regenerative endodontics is particularly challenging, especially biocompatibility of the material, while biodegrad-

**Received:** November 20, 2022

**Accepted:** January 24, 2023

**Published:** February 3, 2023



ability should match the regeneration rate of the pulp tissue, including cellular infiltration, vascularization, differentiation, spatial organization, and replacement of the scaffold.<sup>7</sup> The properties of hydrogels, including biocompatibility, water content, viscoelasticity, transfer efficiency of metabolites and nutrients, degradation rate, distribution of encapsulated cells, injectability, and gelation *in situ* under physiological conditions, must be optimized prior to application in regenerative endodontics.<sup>8–11</sup>

Within the narrow and complex root canal system, injectable biocompatible hydrogels provide a three-dimensional (3D) microstructure to promote cell growth and proliferation.<sup>12,13</sup>

Dental pulp is a nonmineralized soft connective tissue composed of various cell types with a collagen-rich extracellular matrix (ECM), vessels, and nerves. As the scaffold of tissues and organs, the ECM plays important roles in cell differentiation, migration, and proliferation. ECM-like scaffolds are especially important for tissue regeneration. The stiffness of scaffolds influences the behavior of cells through a mechanotransduction mechanism that transforms mechanical stimuli into biochemical signals.<sup>14</sup> Thus, cell behavior can be controlled by regulating the matrix stiffness of the scaffold. A rigid and ductile double-network (DN) structure can effectively adjust the matrix stiffness of hydrogels. However, for pulp regeneration, the DN hydrogel, as an ECM, must be injectable, readily transitional to a gel, and cytocompatible.<sup>15</sup>

In this study, injectable glycol chitosan (GC)-based hydrogels were prepared to promote pulp regeneration. The mechanical properties of the hydrogels were adjusted with and without the formation of a DN structure. The matrix stiffness of a DN hydrogel can be adjusted by changing the composition of chemical components. Three GC-based hydrogels with different degrees of matrix stiffness were formulated, which included a single-network (SN) hydrogel and two DN hydrogels. The biological performance of all three GC-based hydrogels to encapsulate human dental pulp stem cells (hDPSCs) under physiological condition for pulp regeneration was investigated under physiological conditions both *in vitro* and *in vivo*.

## 2. METHODS AND MATERIALS

**2.1. Preparation of Injectable GC-Based SN and DN Hydrogels.** The materials used for the preparation of the hydrogels were purchased from Sigma-Aldrich Corporation (St. Louis, MO). Dibenzaldehyde-capped poly(ethylene oxide) (OHC-PEO-CHO) was synthesized as described in a previous report by our group.<sup>16</sup> An injectable GC-based SN hydrogel was prepared by the Schiff base reaction by mixing 3% GC (w/v) and 1% OHC-PEO-CHO (w/v). The injectable GC-based DN hydrogels were prepared by the Schiff base reaction and ionic crosslinking. The first network was formed with GC and OHC-PEO-CHO, while the second was formed from sodium alginate and calcium chloride (CaCl<sub>2</sub>). One of the DN hydrogels (DN3131) was prepared from 3% GC (w/v), 1% OHC-PEO-CHO (w/v), 3% sodium alginate (w/v), and 1% CaCl<sub>2</sub> (w/v), while a second (DN6262) was prepared from 6% GC (w/v), 2% OHC-PEO-CHO (w/v), 6% sodium alginate (w/v), and 2% CaCl<sub>2</sub> (w/v).

**2.2. Characterization of Injectable GC-Based SN and DN Hydrogels.** **2.2.1. Scanning Electron Microscopy (SEM).** The microscopic structures of the injectable GC-based SN and DN hydrogels were observed with a scanning electron microscope (S-4800; Hitachi High-Technologies Corporation, Tokyo, Japan). Prior to SEM, the samples were washed with deionized water, freeze-dried in liquid nitrogen, and cut into pieces.

**2.2.2. Mechanical Tests.** The tensile strength of the samples (thickness, 1 mm; width, 3 mm; length, 5 mm) was tested using a universal testing machine (model 3367; Instron, Norwood, MA) with a crosshead speed of 10 mm/min until fracture. The tests were conducted in triplicate.

**2.2.3. Flowable Time.** The hydrogels were injected from a dual-syringe kit onto a hydrophilic glass substrate with a slope of 30°. Once the hydrogels no longer flowed, the flowable time was recorded. The experiments were conducted in triplicate.

**2.2.4. Rheology.** The rheological properties of the hydrogels were tested using a rheometer (HAAKE MARS; Thermo Fisher Scientific, Waltham, MA) equipped with a 25 mm parallel plate at a gap distance of 1 mm and a Peltier cell to control the temperature. GC, OHC-PEG-CHO, sodium alginate, and CaCl<sub>2</sub> were mixed to the desired concentrations for 30 s and then poured onto the plate. Time sweep rheology analysis was conducted at 37 °C with a shear strain of 1%, which was predetermined in the linear viscoelastic region. Gel formation occurred when the storage modulus  $G'$  was larger than the loss modulus  $G''$ .

**2.2.5. Degradation of the Transparent Root Canal Model.** This experiment was conducted under conditions mimicking those of the root canal. Standard 10  $\mu$ L pipette tips (Axygen; Corning Incorporated, Corning, NY) were used to simulate the root canal. The components of the hydrogel were loaded into a special dual drug mixing device and injected into the pipette tips. The upper opening of each tip was sealed, and the lower opening was placed in water to simulate the apical foramen at the apex of the tooth root. The hydrogels in the transparent models were observed with an optical microscope (SZ61; Olympus Corporation, Tokyo, Japan) at three time points: immediately after injection and then at 1 and 2 weeks.

**2.3. Observation of 3D Cultures of hDPSCs *In Vitro*.** Cultures of hDPSCs were supplied by Prof. Liu.<sup>17</sup> Fully developed human third molars from patients aged 19–25 years were collected with informed consent for primary culture of hDPSCs. The pulp tissues were isolated and cut into pieces, which were transferred into the wells of six-well plates and digested with 0.3 mg/mL collagenase type I (Sigma-Aldrich Corporation) and 0.4 mg/mL dispase (Sigma-Aldrich Corporation) for 30 min at 37 °C on a horizontal shaker. Enzymatic digestion was terminated by the addition of Dulbecco's modified Eagle's medium (DMEM; Gibco, Grand Island, NY). After centrifugation, the samples were cultured in DMEM supplemented with 20% fetal bovine serum (HyClone Laboratories, Inc., South Logan, UT), 100  $\mu$ g/mL streptomycin, and 100 U/mL penicillin in a CO<sub>2</sub> incubator (Thermo Fisher Scientific) at 37 °C. The hDPSCs were subcultured to 80% confluence. At passage 4, the hDPSCs (density,  $1 \times 10^6$ /mL) were encapsulated with the hydrogels by mixing with the OHC-PEO-CHO solution before sol–gel transition. After culturing for 3 days, the cell-loaded hydrogels were fixed with glutaraldehyde and dehydrated with a gradient series of ethanol solutions. The samples were cut to expose the cross section, and the inner morphology was characterized by SEM. Cell proliferation was assessed with a laser confocal microscope (stimulated emission depletion; Leica Microsystems GmbH, Wetzlar, Germany). Three samples from each group were collected on day 0 and weeks 1 and 2 and stained with the nuclear dye 4',6-diamidino-2-phenylindole (DAPI; ZSGB-BIO, Beijing, China) for cell counting. The ratio of the two DN hydrogels and SN hydrogel was calculated.

**2.4. *In Vitro* Differentiation of hDPSCs in 3D and Two-Dimensional (2D) Cultures.** For the 3D culture, hDPSC-loaded SN and DN hydrogels were prepared as described above and cultured in DMEM supplemented with 10% fetal bovine serum for 1, 2, and 3 weeks. For the 2D culture, hDPSCs were cultured in the six-well plate with odontogenic medium for 1, 2, and 3 weeks. The samples were washed twice with phosphate-buffered saline (PBS). Afterward, the mRNA levels of dentin sialophosphoprotein (DSPP), dentin matrix protein-1 (DMP-1), and alkaline phosphatase (ALP) were detected using an RNeasy Animal RNA Isolation Kit with Spin Column (Beyotime Institute of Biotechnology, Shanghai, China) in accordance with the manufacturer's instructions and reverse-transcribed into complementary DNA using a reverse transcription kit

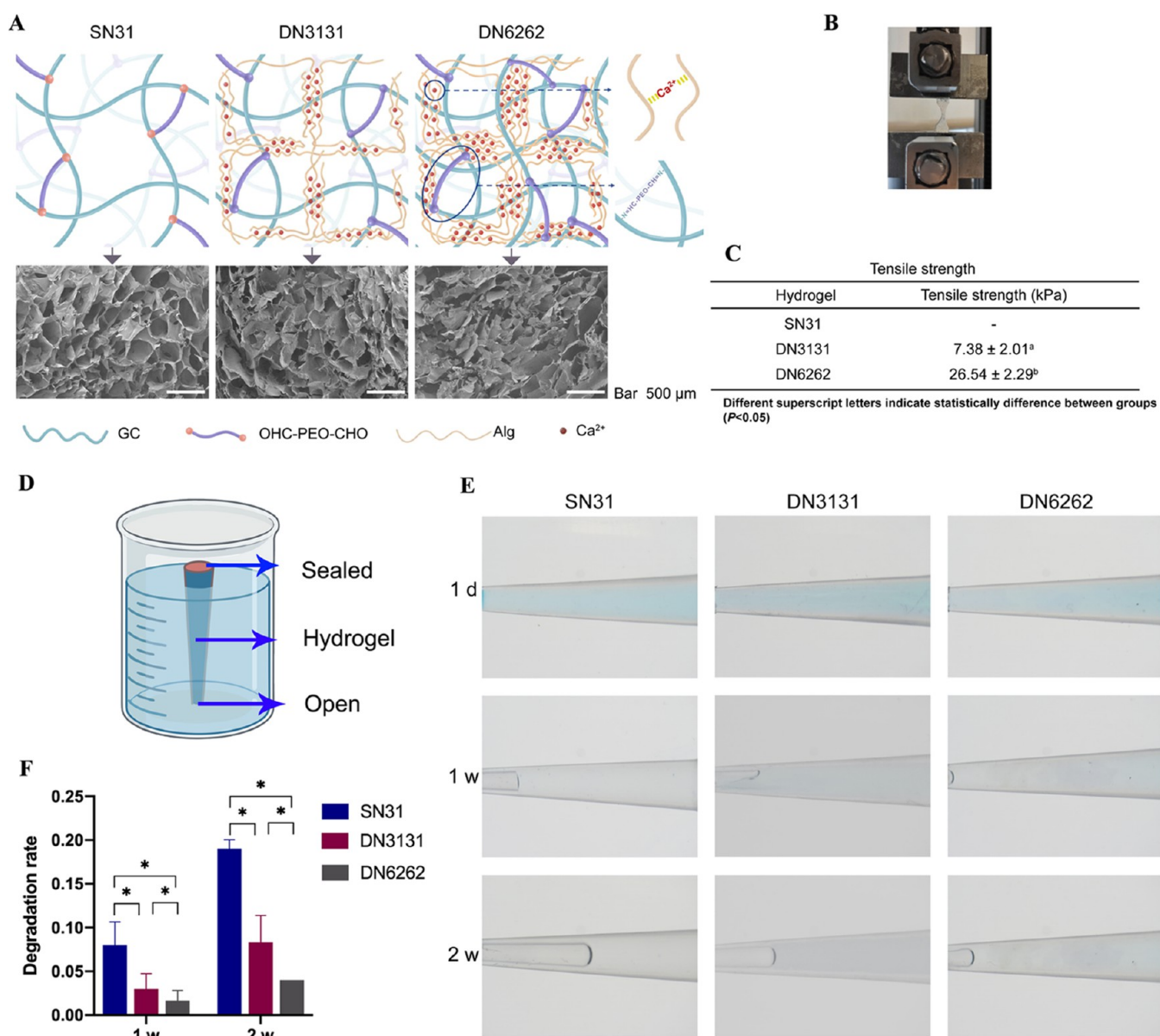


**Figure 1.** Mechanical and physical characterization of the injectable GC-based SN and DN hydrogels. (A) Schematic diagram showing the structures of the GC-based hydrogels (SN31, DN3131, and DN6262), which had loose and porous microstructures. (B) Demonstration of the tensile test. (C) Tensile strength of the hydrogels. Different superscript letters indicate a statistically significant difference between groups ( $p < 0.05$ ). (D) Degradation of the injectable GC-based hydrogels in a transparent root canal model. (E) Degradation of all three GC-based hydrogels after 1 day, 1 week, and 2 weeks. (F) The degradation rate of the SN hydrogel was faster than that of the DN hydrogels in the order SN > DN3131 > DN6262. Each bar represents the mean  $\pm$  standard deviation (SD). \* $p < 0.05$ .

(5 $\times$ PrimeScript RT Master Mix; TaKaRa Bio, Inc., Kusatsu, Japan). Real-time polymerase chain reactions were performed using FastStart Universal SYBR Green Master (Rox) (Roche, Basel, Switzerland) and an Applied Biosystems 7500 Fast Real-Time PCR System (Applied Biosystems, Foster City, CA) with the primer sets (Table S1). Relative mRNA levels were calculated using the  $2^{-\Delta\Delta C_t}$  method against  $\beta$ -actin as an internal control. The protein expression levels of DSPP and DMP-1 after culturing for 2 weeks were observed with a laser confocal microscope (stimulated emission depletion; Leica Microsystems GmbH). Antibodies against DMP-1 (Santa Cruz Biotechnology, Inc., Dallas, TX) and DSPP (Abcam, Cambridge, MA) were used to assess differentiation of odontoblasts *in vitro*.

**2.5. Von Kossa Staining.** SN and DN hydrogels loaded with hDPSCs were prepared as described above and cultured in DMEM supplemented with 10% fetal bovine serum for 2 weeks. Afterward, the samples were fixed with 4% paraformaldehyde, embedded with

paraffin, and cut into 5  $\mu$ m thick sections, which were heated for 2 h at 58  $^{\circ}$ C, deparaffinized in xylene, dehydrated with a gradient series of ethanol solutions, incubated in silver nitrate solution, irradiated with ultraviolet light for 45 min, incubated in 0.1% nuclear solid red dye for 10 min, dehydrated with a gradient series of ethanol solutions, vitrified with dimethylbenzene, dehydrated in alcohol for 2 min, sealed in neutral gum, and observed under a microscope (BX51; Olympus Corporation) equipped with a digital camera (DP72; Olympus Corporation).

**2.6. In Vivo Animal Experiments.** The protocols of all animal studies were approved by the Biomedical Ethics Committee of Peking University School and Hospital of Stomatology (approval no. PKUSSIRB-201943038 and LA2017049) and conducted in accordance with the "Guide for the Care and Use of Laboratory Animals". Fourteen 5 week old male BALB/c nude mice (mean body weight, 20  $\pm$  2 g) were obtained from Beijing Vital River Laboratory Animal

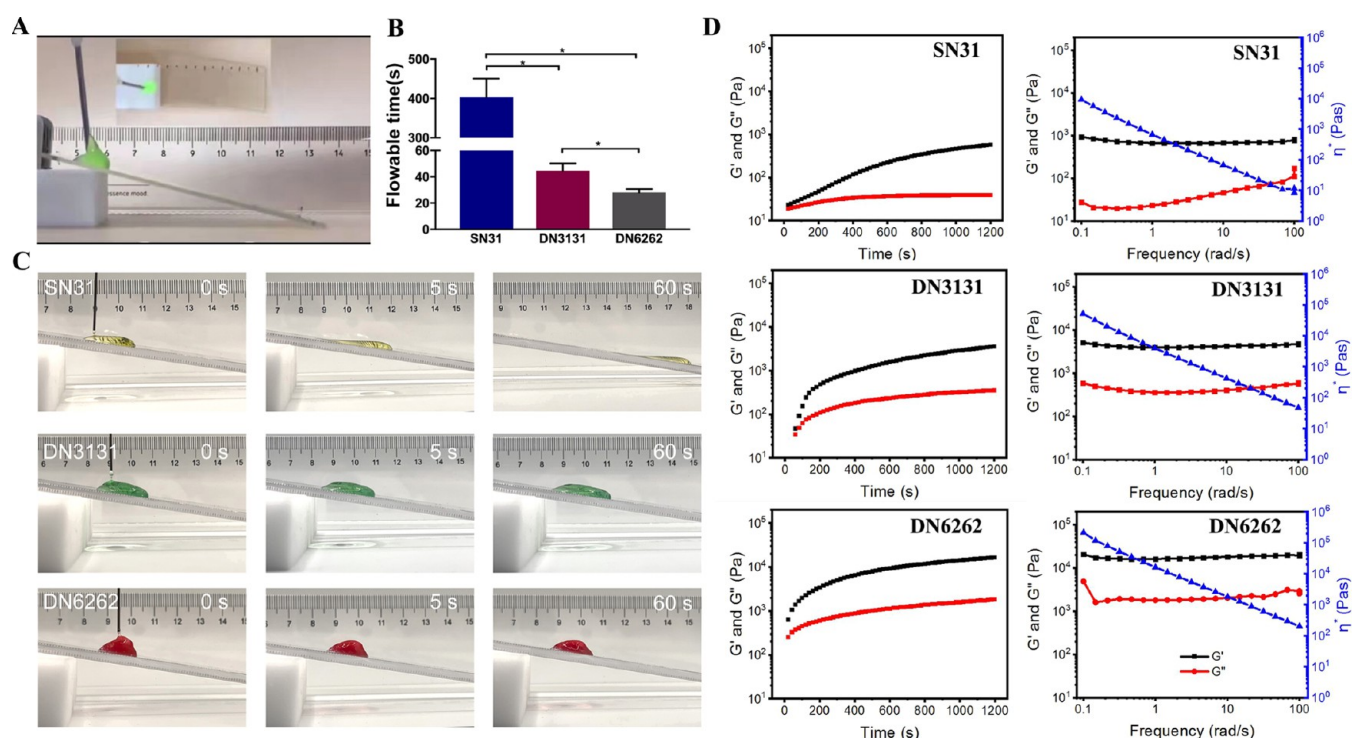


**Figure 2.** Flowable time, time sweeping, and frequency sweeping of the injectable GC-based SN and DN hydrogels. (A) Model to test the flowability of the injectable GC-based hydrogels. (B, C) Calculated gelation times of the DN3131, DN6262, and SN hydrogels were  $44.7 \pm 5.5$ ,  $28.0 \pm 2.6$ , and  $403.3 \pm 47.5$  s, respectively. The differences in flowable time among the samples were statistically significant ( $p < 0.05$ ). (D) Time sweeping and frequency sweeping of the hydrogels. The experiment was performed at  $37^\circ\text{C}$ . For the DN6262 hydrogel,  $G'$  was already higher than  $G''$  from the beginning of the sweeping, indicating that the gelation time was about 30 s sooner after mixing of the components. In contrast, for the DN3131 hydrogel, a cross point of  $G'$  and  $G''$  appeared at 60 s. In addition, the shear moduli of DN6262 were higher than those of DN3131 after gelation. Nonetheless,  $G'$  of DN3131 was as high as  $4 \times 10^3$  Pa. These findings indicate that the injectability of the DN gels can be adjusted by changing the chemical composition.

Technology Co., Ltd. (Beijing, China). Healthy single-rooted teeth were collected and horizontally sectioned into 6 mm long segments as described in a previous study.<sup>18</sup> The root segments (RSs) were cleaned and shaped with a diamond bur to an inner diameter of 2 mm, then soaked in 5.25% sodium hypochlorite solution for 20 min followed by 17% ethylenediaminetetraacetic acid (EDTA) solution for 15 min, washed three times with PBS, and stored in PBS supplemented with  $100 \mu\text{g/mL}$  streptomycin and  $100 \text{ U/mL}$  penicillin at  $4^\circ\text{C}$ . The RSs were randomly allocated to one of the following seven groups: group 1, SN31 hydrogel-encapsulated hDPSC-filled RSs (density,  $1 \times 10^6$  cells/mL); group 2, DN3131 hydrogel-encapsulated hDPSC-filled RSs (density,  $1 \times 10^6$  cells/mL); group 3, DN6262 hydrogel-encapsulated hDPSC-filled RSs (density,  $1 \times 10^6$  cells/mL); group 4, SN31 hydrogel-filled RSs; group 5, DN3131 hydrogel-filled RSs; group 6, DN6262 hydrogel-filled RSs; and group 7, empty RSs. Four replicate samples from each of the seven groups were subcutaneously implanted in nude mice and grown for 6 weeks. Afterward, the RSs of all seven groups were retrieved, fixed in 10% formaldehyde for 48 h, demineralized with EDTA for 4 weeks, and cut into  $5 \mu\text{m}$  thick sections, which were stained with hematoxylin and eosin (H&E) and Masson's trichrome for histological analysis. Immunohistochemical analysis was conducted using human-specific antibodies against DMP-1 (Santa Cruz Biotechnology, Inc.) and DSPP (Abcam) to assess the differentiation of odontoblasts in newly formed pulp-like tissues. Immunofluorescence staining of transforming growth factor (TGF)- $\beta 1$  (Abcam), SMAD family member 3 (Smad3; Abcam), and DAPI (Abcam) was conducted to detect Smad3 activation. A minimum of three slides were produced for each group and observed under a light microscope (Carl Zeiss AG, Jena, Germany).

**2.7. Statistical Analysis.** All statistical analyses were performed using IBM SPSS Statistics for Windows, version 26.0 (IBM

Corporation, Armonk, NY). The significance of differences among groups was determined with one-way analysis of variance. A probability ( $p$ ) value of  $<0.05$  was considered statistically significant.

### 3. RESULTS AND DISCUSSION

**3.1. Preparation and Characterization of Injectable GC-Based SN and DN Hydrogels.** DN hydrogels were formed from compositions, which included GC, OHC-PEO-CHO, sodium alginate, and  $\text{CaCl}_2$ . GC and OHC-PEO-CHO were cross-linked through benzoic-imine linkages to form the first network, while calcium ions were interacted with sodium alginate via electrostatic force to form the second network (Figure 1A). In contrast, the SN hydrogel was composed of GC and OHC-PEO-CHO (Figure 1A). SEM revealed that the microstructures of the freeze-dried hydrogels were generally loose and porous (Figure 1A). Meanwhile, the pores of the SN hydrogel were relatively round, while those of the DN hydrogels were polygonal. Moreover, the tensile strength of the DN6262 hydrogel was greater than those of the DN3131 hydrogel due to a greater crosslink density ( $p < 0.05$ ) (Figure 1B,C), while the tensile strength of SN hydrogel was too weak to measure.

Degradation of the hydrogels in a transparent root canal model is illustrated in Figure 1D–F. All three hydrogels completely filled the canal model, but the degradation rates differed in the order SN31 > DN3131 > DN6262. The slower degradation rate of the DN structure was due to the higher polymer concentrations and subsequent formation of more compact networks and a greater number of crosslink points.

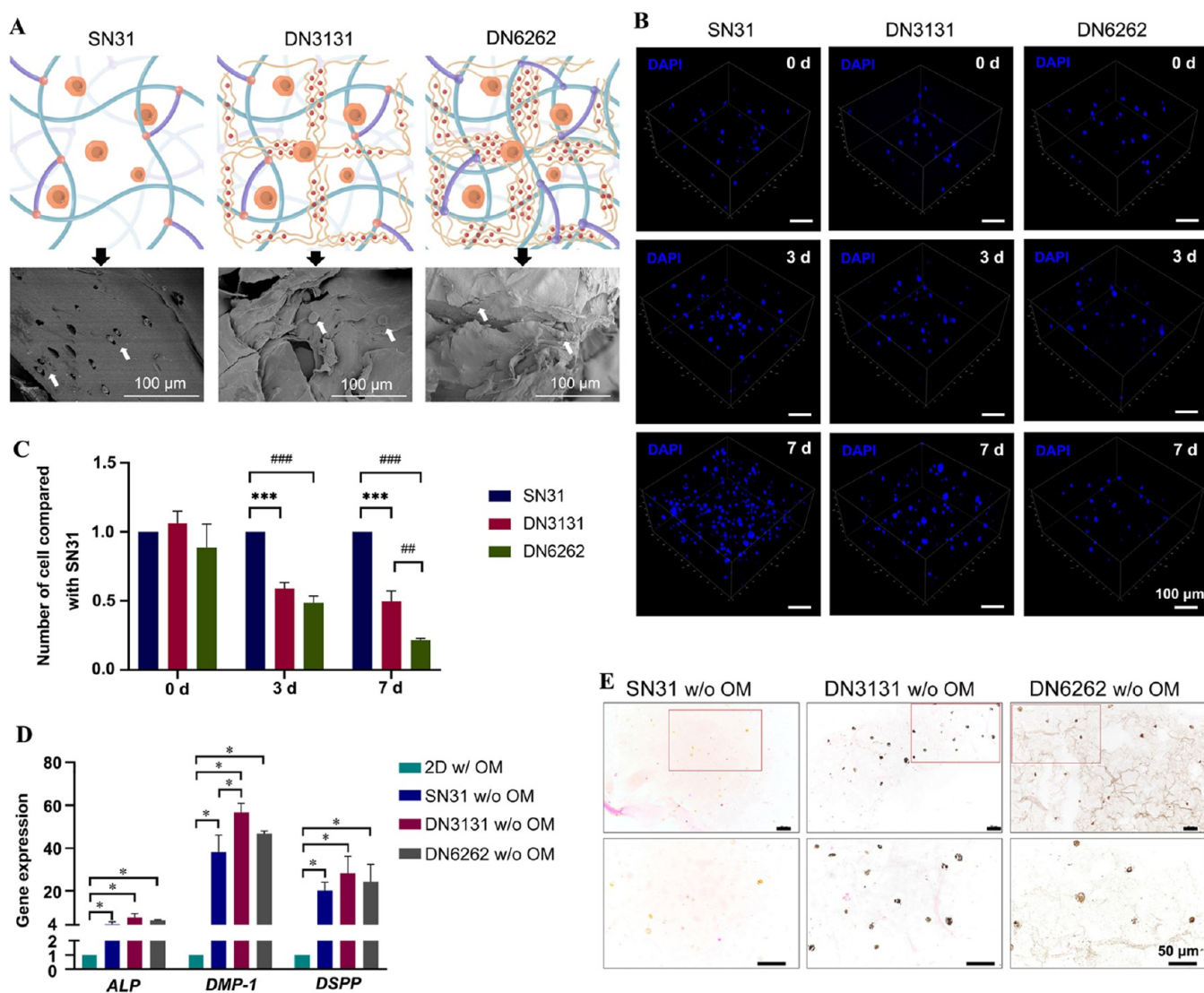


**Figure 3.** Biological performance of hDPSCs cultured in injectable GC-based SN and DN hydrogels *in vitro*. (A) Schematic diagram and SEM images of cells cultured in hydrogels *in vitro*. (B) hDPSCs cultured in three GC-based hydrogels were observed after 1 day, 1 week, and 2 weeks with a confocal laser scanning microscope. (C) Proliferation rate of hDPSCs occurred in the order SN31 > DN3131 > DN6262 ( $p < 0.05$ ). (D) Quantitative determination of the mRNA expression levels of DSPP, DMP-1, and ALP as biomarkers of the odontogenic differentiation of hDPSCs cultured in the GC-based SN and DN hydrogels for 2 weeks. Each bar represents the mean  $\pm$  SD.  $*p < 0.05$ . The mRNA expression levels of DSPP, DMP-1, and ALP were higher in hDPSCs cultured in hydrogels without odontogenic medium versus the 2D culture with odontogenic medium. (E) Von Kossa staining of hDPSCs cultured in the GC-based SN and DN hydrogels without odontogenic medium for 2 weeks. Von Kossa staining demonstrated greater mineralization and formation of mass-shaped mineralized nodules with the DN3131 and DN6262 hydrogels without induction culture, while the SN hydrogel contained light brown calcium deposits that were scattered in granular form.

The Schiff base reaction is widely applied to prepare hydrogels with dynamic covalent bonding. Benzoic-imine is more stable at neutral pH and, thus, allows the use of a linear macromolecular crosslinker, such as OHC-PEG-CHO, for sol-gel transition with multi-amine-containing GC under physiological conditions and favors interpenetration of the alginate network into the hydrogel.<sup>7,19</sup> Besides, hydrogels formed by an *in situ* gelling process allow for effective encapsulation of cells and minimally invasive delivery.<sup>20</sup>

Sequential formation of dynamic covalent and physical crosslinks improved the injectability of the DN hydrogels. To demonstrate this attribute, the DN3131 and DN6262 hydrogels were injected from a dual-syringe kit onto a hydrophilic glass substrate with slope of 30°. As shown in Figure 2A–C, both hydrogels were smoothly extruded from a

17G needle. However, the fluidity differed after injection due to differences in the viscosity of the gelling mixtures. At a lower polymer concentration and fewer crosslinks, the injected DN3131 hydrogel flowed downward on the substrate to about 3 cm away from the initial point after roughly 30 s. In contrast, the DN6262 hydrogel virtually showed no movement within a period of 30 s. The calculated flowable times of the DN3131 and DN6262 hydrogels were  $44.7 \pm 5.5$  and  $28.0 \pm 2.6$  s, respectively. Comparatively, the flowable time of the SN hydrogel was significantly greater at  $403.3 \pm 47.5$  s ( $p < 0.05$ ). In consideration of the operation time, the DN3131 and DN6262 hydrogels are both suitable to fill the complex root canal system.

The gelation transition of the DN hydrogels was examined using a time sweeping test at 37 °C. The results showed that

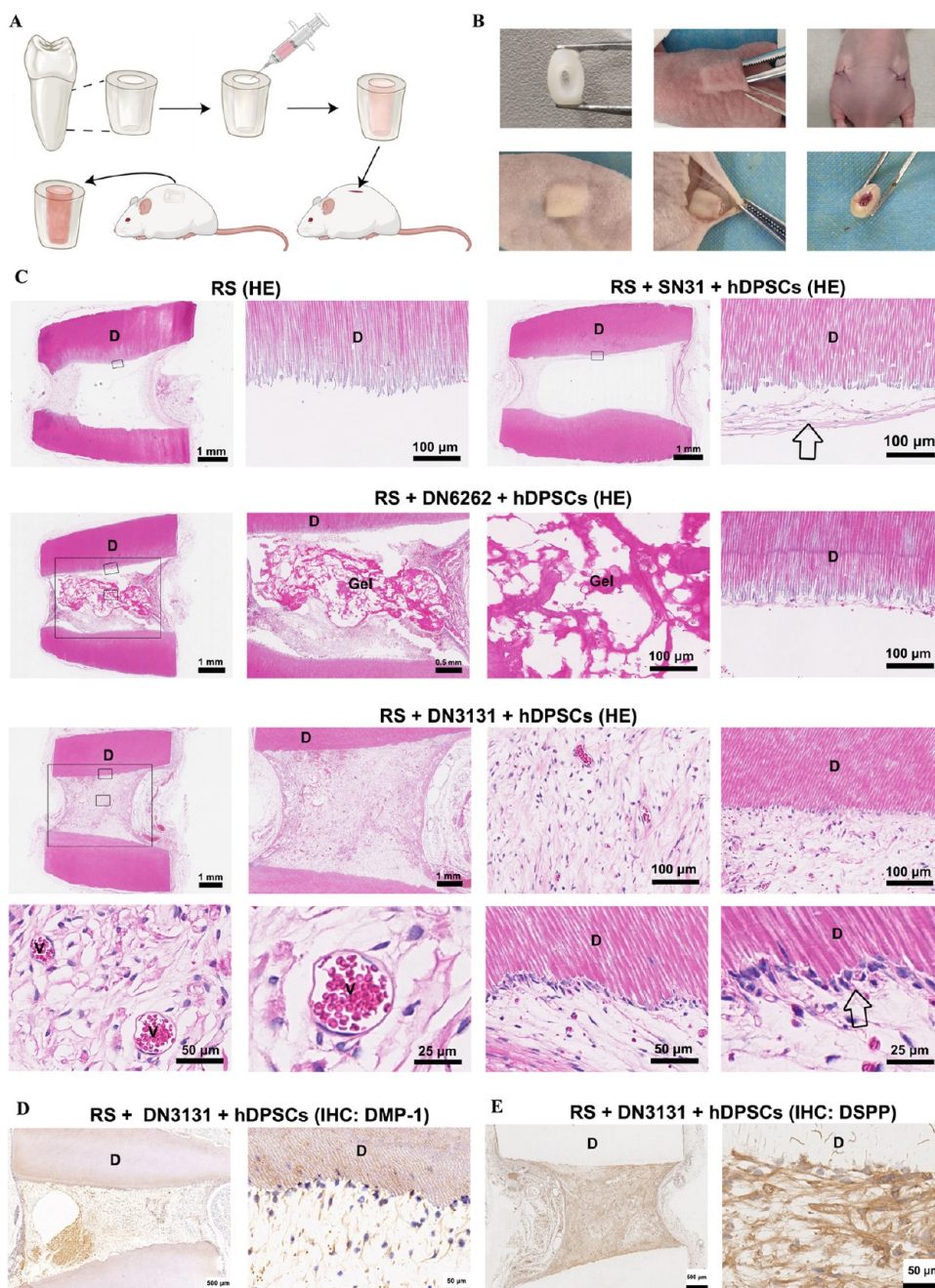


**Figure 4.** 3D culture complex of RS-hydrogel-hDPSCs constructed to investigate the biological performance of hDPSCs encapsulated in the hydrogels *in vivo*. (A) Schematic diagram of subcutaneous implantation in nude mice. (B) Preparation of tooth segments and a schematic diagram of injecting the hydrogel with hDPSCs into the RSs. After 6 weeks of implantation, the complexes were retrieved for further experiments. Representative photos showing the biocompatibility of the SN and DN hydrogels *in vivo*. (C) Pulp regeneration performances of the 3D culture complexes *in vivo*, as evaluated by H&E staining. D: dentin, V: vessel, Gel: hydrogel. Empty RSs as blank controls failed to regenerate pulp tissue. The RS–SN31–hDPSCs complex promoted the formation of small amounts of newly regenerated tissues (black arrows). The DN6262 hydrogels in the RS–DN6262–hDPSCs complex degraded slowly, which hindered generation of new tissues. The RS–DN3131–hDPSCs complex promoted the formation of pulp-like tissues that contained small blood vessels. The hDPSCs near the dentin of the RS–DN3131–hDPSCs complex were arranged in a more orderly manner and even extended into the dentin tubule-like odontoblast layer (black arrows). (D) Odontogenic differentiation marker DMP-1 was detected in the newly regenerated tissue, especially near the dentin. (E) Odontogenic differentiation marker DSPP was detected in the newly regenerated tissue, especially near the dentin.

for the DN6262 hydrogel,  $G'$  was greater than  $G''$  from the beginning of the sweeping, indicating that the gelation time was about 30 s sooner after mixing the components. In contrast, for the DN3131 hydrogel, there was a cross point of  $G'$  and  $G''$  at 60 s (Figure 2D). In addition, the shear moduli of the DN6262 hydrogel were also greater than those of the

DN3131 hydrogel after gelation. Nonetheless, the  $G'$  of the DN3131 hydrogel was as high as  $4 \times 10^3$  Pa (Figure 2D). These findings indicate that the injectability of the DN gels can be adjusted by changing the chemical composition. Pulp regeneration requires the hydrogel to have both fluidity during injection and integrity after implantation.

These results indicate that the fluidity and integrity of the DN hydrogels are adjustable by simply varying the chemical composition. Controlling the physical and mechanical properties of hydrogels provides a unique opportunity to investigate the biological responses of hDPSCs both *in vitro* and *in vivo*,<sup>21</sup> as demonstrated below.

### 3.2. Biological Performance of hDPSCs Encapsulated in Injectable GC-Based SN and DN Hydrogels *In Vitro*.

The hDPSCs encapsulated in the hydrogels appeared spherical (Figures 3A and S2). All three of the hydrogels enabled *in situ* encapsulation, proliferation, and differentiation of the hDPSCs. The injectable hydrogels provided 3D arrangements of the hDPSCs, which mimicked *in vivo* conditions. These 3D culture systems have been previously used to encapsulate human vascular endothelial cells, bone-marrow-derived mesenchymal stem cells, and mouse ATDC5 cells.<sup>15,22</sup> The proliferation rate of hDPSCs in the hydrogels occurred in the order SN31 > DN3131 > DN6262 (Figure 3B,C). A previous report noted that the stiffness of the substrate influenced cell proliferation.<sup>23</sup> According to a previous study, extracellular matrix stiffness could be transmitted to cells as a mechanical stimulus signal, affecting the contraction of the cytoskeleton and the opening of the mitotic pathway of cells, thus affecting proliferative behavior.<sup>23,24</sup> The double-network hydrogel has a higher density of molecular chains. As the concentration of cross-linked molecules increases, extracellular matrix stiffness increases, and the proliferation of cells is correspondingly slowed down. This is consistent with previous studies.<sup>25,26</sup>

The mRNA expression levels of DSPP, DMP-1, and ALP were relatively increased in hDPSCs cultured in hydrogels without odontogenic medium compared to the 2D culture with odontogenic medium ( $p < 0.05$ ) (Figures 3D, S4, and S5). These results indicate that the 3D culture promoted odontogenic differentiation and mineralization of hDPSCs. After 2 weeks, the mRNA expression levels of DSPP, DMP-1, and ALP were relatively higher in the DN hydrogels than the SN hydrogel. The highest mRNA expression levels of DSPP, DMP-1, and ALP occurred in hDPSCs cultured in the DN3131 hydrogel. Von Kossa staining demonstrated greater mineralization and formation of mass-shaped mineralized nodules with the DN3131 and DN6262 hydrogels without induction culture, while the SN hydrogel contained light brown calcium deposits that were scattered in granular form (Figure 3E). Immunofluorescence staining of odontogenic marker DSPP and DMP-1 in hDPSCs cultured in the hydrogels were observed after 2 weeks (Figures S6 and S7). Under 3D cell culture conditions without induction, odontogenic differentiation and mineralization were increased compared to the 2D cell culture conditions. Notably, a 2D cell culture does not reflect the complex microenvironment of cells in tissues and organs. In contrast, a 3D cell culture provides a microenvironment that more closely resembles *in vivo* conditions.<sup>27,28</sup> Under 3D culture conditions, the cells will secrete components of the ECM, which then regulates cell proliferation, differentiation, and migration. The stiffness of the hydrogel affects the biological behaviors of hDPSCs, such as proliferation, odontogenic differentiation, and mineralization. *In vitro*, reduced stiffness of the ECM could improve the proliferative capability of hDPSCs, while increased stiffness may be beneficial to odontogenic differentiation and mineralization. The capacity to regulate the mechanical properties of the hydrogel allows for adjustments of cellular activities.<sup>21</sup> It has been found that at higher matrix stiffness, the

cytoskeleton is more ordered and tends to generate mineralized tissues, whereas at lower matrix stiffness, it tends to generate dental pulp-like soft tissues.<sup>29</sup> However, we also need to take into account the proliferation behavior and survival of hDPSCs in hydrogels. In hydrogels with higher matrix stiffness, cell survival may be limited due to limited space. We hope to select hydrogel culture systems with relatively higher stiffness to facilitate odontogenic differentiation, while ensuring that cells can proliferate and differentiation. All in all, characteristic stiffness of hydrogel scaffolds should satisfy the physiological demands in a cell/tissue type-dependent manner. It is reported that the elastic modulus of the brain, muscle, and bone is 1, 10, and 100 kPa, respectively.<sup>30</sup> According to a previous study, the compressive modulus value of pulp tissue is  $5.5 \pm 2.8$  kPa.<sup>31</sup> The modulus of DN3131 was selected within this range.

### 3.3. Biological Performance of hDPSCs Encapsulated in Injectable GC-Based SN and DN Hydrogels *In Vivo*.

In this study, BALB/c nude mice were selected as an *in vivo* model of subcutaneous ectopic implantation to avoid immune rejection of the grafts. Previous studies of ectopic implantation employed dentin slices, 1 mm thick dentin rings, and 6 mm long RSs.<sup>32</sup> In the present study, 6 mm long RSs were used to better simulate the narrow root canal and the endodontic dentin environment in the ectopic subcutaneous tissue as much as possible (Figure 4A).

A 3D culture of the RS-hydrogel-hDPSCs complex was constructed to observe the biological performance of hDPSCs encapsulated in the hydrogels *in vivo* (Figure 4B). At 6 weeks after subcutaneous implantation in nude mice, there was no inflammatory reaction in the surrounding tissues and blood vessels grew into the hydrogel. The biocompatibility of the SN and DN hydrogels *in vivo* was observed (Figure 4B). Empty RSs as a blank control failed to induce tissue regeneration (Figure 4C). When subcutaneously implanted in nude mice, the RS-hydrogel complexes without hDPSCs also failed to induce tissue regeneration (Figure S8). Meanwhile, the RS–SN-hDPSCs complex quickly degraded and the root canal was nearly empty (Figure 4C). In contrast, the RS–DN6262-hDPSC complex slowly degraded, which hindered the generation of new tissues (Figure 4C). In degradable scaffold materials, it is critical to match the rate of scaffold degradation with the rate of tissue generation,<sup>33</sup> that is, to enable endogenous synthetic extracellular matrix to gradually replace exogenously implanted extracellular matrix. It was found that hDPSCs in DN6262 hydrogel proliferated slowly *in vitro*, which is also an important reason for the difficulty of regeneration in this group. The degradation rate of the DN3131 hydrogel matched the regeneration rate of the RS–DN3131-hDPSC complex, and the root canal was filled with a pulp-like regenerated fibrous connective tissue (Figure 4C). Newly formed small blood vessels were observed in the center of the regenerated tissues (Figure 4C). Revascularization is crucial to provide oxygen and nutrients to cells during the endodontic regeneration process.<sup>34</sup> The cells near the dentin of the RS–DN3131-hDPSC complex were arranged in a more orderly manner, similar to the odontoblast layer (Figure 4C). The layer of newly formed odontoblast-like cells was lined up along the dentin, and cellular processes were inserted into the dentinal tubules (Figure 4C). Immunohistochemical staining showed that hDPSCs near the dentin side highly expressed DMP-1 and DSPP (Figure 4D,E). DMP-1 is a member of the SIBLING protein family that plays important roles in the

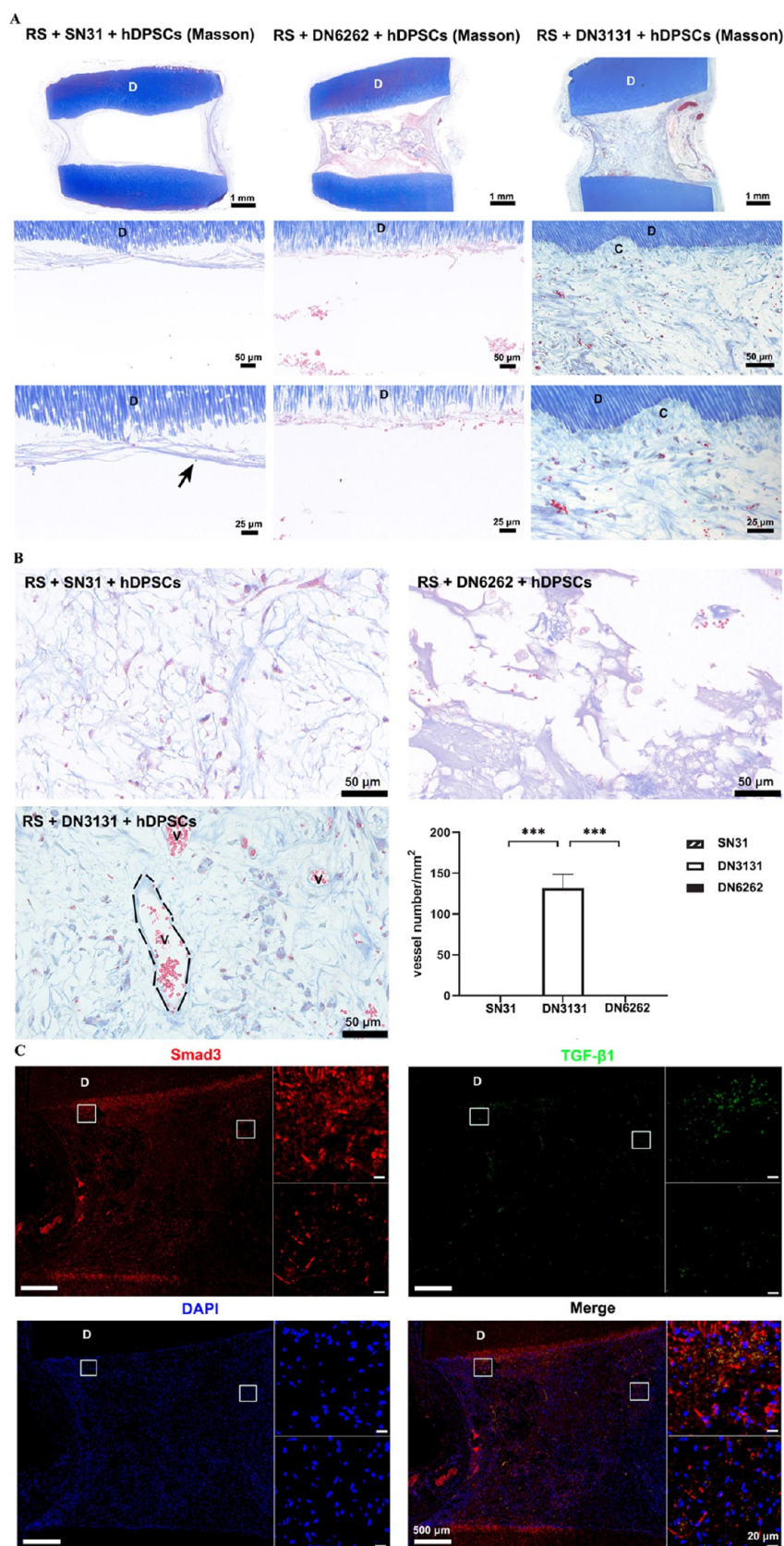


**Figure 5.** The 3D RS-hydrogel-hDPSCs complex was observed with Masson's trichrome staining and immunofluorescence co-staining. (A) Small amounts of collagen I (black arrows) were observed in the RS-SN31-hDPSCs complex, but not the RS-DN6262-hDPSCs complex. Newly formed collagen I was observed with Masson's trichrome staining of the RS-DN3131-hDPSCs complex. Collagen I is the main ECM component of pulp tissue. (B) Observations of newly formed small blood vessels of the three groups. (C) Immunofluorescence co-staining of TGF- $\beta$ 1 and Smad3 in the RS-DN3131-hDPSCs complex. D: dentin, V: vessel.

mineralization and formation of the dentin-pulp complex. DSPP is also a member of SIBLING protein family that is highly expressed in odontoblasts and dentine.<sup>35</sup> Odontogenic differentiation of hDPSCs in the RS-DN3131-hDPSC complex was increased close to the dentin wall.<sup>36</sup> Collagen I is the main ECM component of pulp tissue. A large quantity of newly formed collagen I was observed by Masson's trichrome staining of the RS-DN3131-hDPSC complex (Figure 5A). Newly formed small blood vessels were only observed in the RS-DN3131-hDPSC complex (Figure 5B).

As we all know, cells could sense the mechanical stimulation of the extracellular environment through the mechanical receptors on the cell membrane like integrins and focal adhesion kinases (FAKs), and convert this mechanical signal into biochemical signals, which are transmitted to the nucleus, affecting the biological behavior of cells, such as proliferation, differentiation, survival, migration, etc. The process of cells converting exogenous mechanical signals into biochemical signals is called mechanical transduction.<sup>37</sup> To better understand the mechanisms underlying the regeneration of pulp-like tissue in the RS-DN3131-hDPSC complex, the associated molecular pathways were identified by immunofluorescence staining (Figure 5C). The results revealed expression of TGF- $\beta$ 1 and relatively high expression of Smad3 in the newly formed tissue. These observations suggest that the TGF- $\beta$ 1/Smad3 pathway is activated during the regeneration of pulp-like tissue. The receptor-activated Smad3 protein of the TGF- $\beta$ 1/Smad3 signaling pathway is involved in cell proliferation, differentiation, and migration; ECM remodeling; collagen accumulation; and angiogenesis, which are necessary for pulp regeneration.<sup>38,39</sup> An *in vivo* study on the formation of reparative dentin found that TGF- $\beta$ 1 could promote the formation of reparative dentin by activating Smad2/3 and regulating the transcription of DSP and BSP in odontoblast-like cells.<sup>40</sup> TGF- $\beta$ 1 is also a growth factor that plays an important role in the process of tissue repair after injury, which could promote the deposition of collagen and the formation of extracellular matrix.<sup>41</sup> The disorder of TGF- $\beta$ 1 activation is the pathological basis of some fibrosis diseases.<sup>42</sup> It was demonstrated that mechanical transduction could have extensive crosstalk with TGF- $\beta$  pathway, and external mechanical stimulus could regulate the activation of TGF- $\beta$  pathway.<sup>43,44</sup> When Integrin  $\alpha$ v $\beta$ 6 bound to the RGD site on latency-associated peptide (LAP) in extracellular environment, active TGF- $\beta$  would be released from TGF- $\beta$  LAP and then bound to TGF- $\beta$  receptor. It was speculated that mechanical force was needed during this process to induce the interaction among integrin, actin, and myosin.<sup>45</sup> It had also been found that stiffness affected the differentiation of corneal cells into myofibroblasts mediated by TGF- $\beta$ 1 through the activity of FAK, a signal molecule downstream of focal adhesion complex.<sup>46</sup> A study of renal fibroblasts showed that the change of matrix stiffness regulated the phosphorylation and nuclear localization of Smad2/3, and the way involved the relative change of YAP/TAZ activity.<sup>47</sup> All in all, some evidence showed that there is considerable crosstalk between the mechanical transduction pathway and TGF- $\beta$ /Smad2/3 signaling.<sup>43,47–49</sup> These results demonstrate that the DN3131 hydrogel matched the regeneration of pulp-like fibrous connective tissue, in terms of composition, matrix stiffness, and degradation rate, and that activation of TGF- $\beta$ 1/Smad3 signaling pathway may be involved in the regeneration process. The mechanism of matrix stiffness on the biological behaviors

of cells and the activation of cascades related with mechano-transduction will be the focus of our future study.

## 4. CONCLUSIONS

Injectable hydrogel-based 3D cell culture systems under physiological conditions for dental pulp regeneration enabled *in situ* encapsulation, proliferation, and differentiation of cells. The DN hydrogels with polysaccharides through the formation of dynamic covalent and physical crosslinks had much improved mechanical property that can be regulated via crosslink density. Within the hydrogels without odontogenic medium, the hDPSCs were uniformly encapsulated and expressed relatively high mRNA levels of DSPP, DMP-1, and ALP compared to 2D culture conditions with odontogenic medium. The 3D culture conditions promoted odontogenic differentiation and mineralization of hDPSCs but varied due to the differences in the physical and mechanical properties of the hydrogels. The DN3131 hydrogel exhibited the highest odontogenic differentiation and mineralization expression *in vitro* and contributed to the regeneration of pulp-like tissue with an appropriate degradation rate *in vivo*. DMP-1, DSPP, and Collagen I were detected in the regenerated tissue. New small blood vessels formed in the regenerated tissue, which promoted tissue regeneration in return. The regeneration process might be related to Smad3 activation. The injectable DN hydrogels have great potential for the regeneration of pulp tissue.

## ■ ASSOCIATED CONTENT

### Data Availability Statement

Data will be made available on request.

### SI Supporting Information

The Supporting Information is available free of charge at <https://pubs.acs.org/doi/10.1021/acsami.2c20848>.

Quantitative determination of mRNA expression of odontogenic differentiation marker genes (DSPP, DMP-1 and ALP) for hDPSCs in the 2D culture condition with or without odontogenic medium for 1, 2, and 3 weeks (Figure S1); observation of the hDPSCs encapsulated in GC-based hydrogel by inverted microscope after cultured for 3 days and 7 days (Figure S2); immunofluorescence staining of Actin (green) in hDPSCs cultured in the GC-based SN and DN hydrogels at 0, 3, and 14 days (Figure S3); quantitative determination of mRNA expression of odontogenic differentiation marker genes (DSPP, DMP-1, and ALP) for hDPSCs cultured in the GC-based SN and DN hydrogels for 1 week (Figure S4); quantitative determination of mRNA expression of odontogenic differentiation marker genes (DSPP, DMP-1, and ALP) for hDPSCs cultured in the GC-based SN and DN hydrogels for 3 weeks (Figure S5); immunofluorescence staining of odontogenic marker DMP-1 (green) in hDPSCs cultured in the GC-based SN and DN hydrogels at 14 days (Figure S6); immunofluorescence staining of odontogenic marker DSPP (red) in hDPSCs cultured in the GC-based SN and DN hydrogels at 14 days (Figure S7); the pulp regeneration performances of complexes without hDPSCs evaluated using H&E staining *in vivo* (Figure S8); and sequences of forward and reverse primers for q-PCR (Table S1) (PDF)

## AUTHOR INFORMATION

### Corresponding Authors

**Zhenzhong Yang** – Department of Chemical Engineering, Tsinghua University, Beijing 100084, China; [orcid.org/0000-0002-4810-7371](https://orcid.org/0000-0002-4810-7371); Email: [yangzhenzhong@tsinghua.edu.cn](mailto:yangzhenzhong@tsinghua.edu.cn)

**Xiaozhong Qu** – College of Materials Science and Optoelectronic Technology, University of Chinese Academy of Sciences, Beijing 100049, China; [orcid.org/0000-0002-4050-6079](https://orcid.org/0000-0002-4050-6079); Email: [quxz@iccas.ac.cn](mailto:quxz@iccas.ac.cn)

**Xiaoyan Wang** – Department of Cariology and Endodontology, Peking University School and Hospital of Stomatology & National Center of Stomatology & National Clinical Research Center for Oral Diseases & National Engineering Laboratory for Digital and Material Technology of Stomatology & Beijing Key Laboratory of Digital Stomatology & Research Center of Engineering and Technology for Computerized Dentistry Ministry of Health & NMPA Key Laboratory for Dental Materials, Beijing 100081, China; [orcid.org/0000-0002-8763-289X](https://orcid.org/0000-0002-8763-289X); Email: [wangxiaoyan@pkuss.bjmu.edu.cn](mailto:wangxiaoyan@pkuss.bjmu.edu.cn)

### Authors

**Bing Han** – Department of Cariology and Endodontology, Peking University School and Hospital of Stomatology & National Center of Stomatology & National Clinical Research Center for Oral Diseases & National Engineering Laboratory for Digital and Material Technology of Stomatology & Beijing Key Laboratory of Digital Stomatology & Research Center of Engineering and Technology for Computerized Dentistry Ministry of Health & NMPA Key Laboratory for Dental Materials, Beijing 100081, China

**Chunling Cao** – Department of Cariology and Endodontology, Peking University School and Hospital of Stomatology & National Center of Stomatology & National Clinical Research Center for Oral Diseases & National Engineering Laboratory for Digital and Material Technology of Stomatology & Beijing Key Laboratory of Digital Stomatology & Research Center of Engineering and Technology for Computerized Dentistry Ministry of Health & NMPA Key Laboratory for Dental Materials, Beijing 100081, China

**Aijing Wang** – Department of Cariology and Endodontology, Peking University School and Hospital of Stomatology & National Center of Stomatology & National Clinical Research Center for Oral Diseases & National Engineering Laboratory for Digital and Material Technology of Stomatology & Beijing Key Laboratory of Digital Stomatology & Research Center of Engineering and Technology for Computerized Dentistry Ministry of Health & NMPA Key Laboratory for Dental Materials, Beijing 100081, China

**Yanran Zhao** – College of Materials Science and Optoelectronic Technology, University of Chinese Academy of Sciences, Beijing 100049, China

**Moran Jin** – Department of Cariology and Endodontology, Peking University School and Hospital of Stomatology & National Center of Stomatology & National Clinical Research Center for Oral Diseases & National Engineering Laboratory for Digital and Material Technology of Stomatology & Beijing Key Laboratory of Digital Stomatology & Research Center of Engineering and

Technology for Computerized Dentistry Ministry of Health & NMPA Key Laboratory for Dental Materials, Beijing 100081, China

**Yuhan Wang** – Department of Cariology and Endodontology, Peking University School and Hospital of Stomatology & National Center of Stomatology & National Clinical Research Center for Oral Diseases & National Engineering Laboratory for Digital and Material Technology of Stomatology & Beijing Key Laboratory of Digital Stomatology & Research Center of Engineering and Technology for Computerized Dentistry Ministry of Health & NMPA Key Laboratory for Dental Materials, Beijing 100081, China

**Shuqin Chen** – Department of Cariology and Endodontology, Peking University School and Hospital of Stomatology & National Center of Stomatology & National Clinical Research Center for Oral Diseases & National Engineering Laboratory for Digital and Material Technology of Stomatology & Beijing Key Laboratory of Digital Stomatology & Research Center of Engineering and Technology for Computerized Dentistry Ministry of Health & NMPA Key Laboratory for Dental Materials, Beijing 100081, China

**Min Yu** – Department of Orthodontics, Peking University School and Hospital of Stomatology & National Center of Stomatology & National Clinical Research Center for Oral Diseases & National Engineering Laboratory for Digital and Material Technology of Stomatology & Beijing Key Laboratory of Digital Stomatology & Research Center of Engineering and Technology for Computerized Dentistry Ministry of Health & NMPA Key Laboratory for Dental Materials, Beijing 100081, China

Complete contact information is available at: <https://pubs.acs.org/10.1021/acsami.2c20848>

### Author Contributions

<sup>†</sup>B.H. and C.C. contributed equally to this work. B.H.: conducted the experiments and drafted the manuscript. C.C.: conducted the experiments and drafted the manuscript. A.W.: conducted the experiment of proliferation of hDPSCs. Y.Z.: conducted the time sweeping and frequency sweeping of the hydrogels. M.J.: contributed to laboratory research of degradation of GC-based SN and DN hydrogels. Y.W.: contributed to laboratory research of degradation of GC-based SN and DN hydrogels. S.C.: contributed to laboratory research of degradation of GC-based SN and DN hydrogels. M.Y.: contributed to laboratory research of mechanisms underlying the regeneration of pulp-like tissue *in vivo*. Z.Y.: designed the experiment and reviewed the article. X.Q.: designed the experiment and reviewed the article. X.W.: designed the experiment and reviewed the article.

### Notes

The authors declare no competing financial interest. The authors declare that they have no known competing financial interests or personal relationships that could have appeared to influence the work reported in this paper.

## ACKNOWLEDGMENTS

This research was supported by the National Natural Science Foundation of China (81771061, 52273062).

## REFERENCES

- (1) Friedman, P. K.; Lamster, I. B. Tooth Loss as a Predictor of Shortened Longevity: Exploring the Hypothesis. *Periodontol.* **2000** *2016*, *72*, 142–152.
- (2) Thompson, V. P. The Tooth: An Analogue for Biomimetic Materials Design and Processing. *Dent. Mater.* **2020**, *36*, 25–42.
- (3) Madl, C. M.; Heilshorn, S. C.; Blau, H. M. Bioengineering Strategies to Accelerate Stem Cell Therapeutics. *Nature* **2018**, *557*, 335–342.
- (4) Langer, R.; Vacanti, J. P. Tissue Engineering. *Science* **1993**, *260*, 920–926.
- (5) Itoh, Y.; Sasaki, J. I.; Hashimoto, M.; Katata, C.; Hayashi, M.; Imazato, S. Pulp Regeneration by 3-Dimensional Dental Pulp Stem Cell Constructs. *J. Dent. Res.* **2018**, *97*, 1137–1143.
- (6) Dissanayaka, W. L.; Zhang, C. Scaffold-Based and Scaffold-Free Strategies in Dental Pulp Regeneration. *J. Endod.* **2020**, *46*, S81–S89.
- (7) Xu, J.; Liu, Y.; Hsu, S. H. Hydrogels Based on Schiff Base Linkages for Biomedical Applications. *Molecules* **2019**, *24*, 3005.
- (8) Goldberg, M. *The Dental Pulp: Biology, Pathology, and Regenerative Therapies*; Springer, 2014.
- (9) Divband, B.; Aghazadeh, M.; Al-Qaim, Z. H.; Samiei, M.; Hussein, F. H.; Shaabani, A.; Shahi, S.; Sedghi, R. Bioactive Chitosan Biguanidine-Based Injectable Hydrogels as a Novel Bmp-2 and Vegf Carrier for Osteogenesis of Dental Pulp Stem Cells. *Carbohydr. Polym.* **2021**, *273*, No. 118589.
- (10) Han, X.; Tang, S.; Wang, L.; Xu, X.; Yan, R.; Yan, S.; Guo, Z.; Hu, K.; Yu, T.; Li, M.; Li, Y.; Zhang, F.; Gu, N. Multicellular Spheroids Formation on Hydrogel Enhances Osteogenic/Odontogenic Differentiation of Dental Pulp Stem Cells under Magnetic Nanoparticles Induction. *Int. J. Nanomed.* **2021**, *Volume 16*, 5101–5115.
- (11) Atila, D.; Chen, C. Y.; Lin, C. P.; Lee, Y. L.; Hasirci, V.; Tezcaner, A.; Lin, F. H. In Vitro Evaluation of Injectable Tideglusib-Loaded Hyaluronic Acid Hydrogels Incorporated with Rg1-Loaded Chitosan Microspheres for Vital Pulp Regeneration. *Carbohydr. Polym.* **2022**, *278*, No. 118976.
- (12) Dissanayaka, W. L.; Hargreaves, K. M.; Jin, L.; Samaranyake, L. P.; Zhang, C. The Interplay of Dental Pulp Stem Cells and Endothelial Cells in an Injectable Peptide Hydrogel on Angiogenesis and Pulp Regeneration in Vivo. *Tissue Eng., Part A* **2015**, *21*, 550–563.
- (13) d'Angelo, M.; Benedetti, E.; Tupone, M. G.; Catanesi, M.; Castelli, V.; Antonosante, A.; Cimini, A. The Role of Stiffness in Cell Reprogramming: A Potential Role for Biomaterials in Inducing Tissue Regeneration. *Cells* **2019**, *8*, 1036.
- (14) Bottino, M. C.; Pankajakshan, D.; Nör, J. E. Advanced Scaffolds for Dental Pulp and Periodontal Regeneration. *Dent. Clin. North Am.* **2017**, *61*, 689–711.
- (15) Yang, C.; Han, B.; Cao, C.; Yang, D.; Qu, X.; Wang, X. An Injectable Double-Network Hydrogel for the Co-Culture of Vascular Endothelial Cells and Bone Marrow Mesenchymal Stem Cells for Simultaneously Enhancing Vascularization and Osteogenesis. *J. Mater. Chem. B* **2018**, *6*, 7811–7821.
- (16) Zhu, F.; Wang, C.; Yang, S.; Wang, Q.; Liang, F.; Liu, C.; Qiu, D.; Qu, X.; Hu, Z.; Yang, Z. Injectable Tissue Adhesive Composite Hydrogel with Fibroblasts for Treating Skin Defects. *J. Mater. Chem. B* **2017**, *5*, 2416–2424.
- (17) Cui, S.-J.; Fu, Y.; Yu, M.; Zhang, L.; Zhao, W.-Y.; Zhang, T.; Qiu, L.-X.; Gu, Y.; Zhou, Y.-H.; Liu, Y. Functional Periodontal Regeneration Using Biomaterialized Extracellular Matrix/Stem Cell Microspheroids. *Chem. Eng. J.* **2022**, *431*, No. 133220.
- (18) Khayat, A.; Monteiro, N.; Smith, E. E.; Pagni, S.; Zhang, W.; Khademhosseini, A.; Yelick, P. C. Gelma-Encapsulated Hdpscs and Huvecs for Dental Pulp Regeneration. *J. Dent. Res.* **2017**, *96*, 192–199.
- (19) Yu, F.; Cao, X.; Du, J.; Wang, G.; Chen, X. Multifunctional Hydrogel with Good Structure Integrity, Self-Healing, and Tissue-Adhesive Property Formed by Combining Diels-Alder Click Reaction and Acylhydrazone Bond. *ACS Appl. Mater. Interfaces* **2015**, *7*, 24023–24031.
- (20) Dimatteo, R.; Darling, N. J.; Segura, T. In Situ Forming Injectable Hydrogels for Drug Delivery and Wound Repair. *Adv. Drug Delivery Rev.* **2018**, *127*, 167–184.
- (21) Abdallah, M.; Martin, M.; El Tahchi, M. R.; Balme, S.; Faour, W. H.; Varga, B.; Cloitre, T.; Páll, O.; Cuisinier, F. J. G.; Gergely, C.; Bassil, M. J.; Bechelany, M. Influence of Hydrolyzed Polyacrylamide Hydrogel Stiffness on Podocyte Morphology, Phenotype, and Mechanical Properties. *ACS Appl. Mater. Interfaces* **2019**, *11*, 32623–32632.
- (22) Yan, Y.; Li, M.; Yang, D.; Wang, Q.; Liang, F.; Qu, X.; Qiu, D.; Yang, Z. Construction of Injectable Double-Network Hydrogels for Cell Delivery. *Biomacromolecules* **2017**, *18*, 2128–2138.
- (23) Janmey, P. A.; Miller, R. T. Mechanisms of Mechanical Signaling in Development and Disease. *J. Cell Sci.* **2011**, *124*, 9–18.
- (24) Chen, C. S.; Mrksich, M.; Huang, S.; Whitesides, G. M.; Ingber, D. E. Geometric Control of Cell Life and Death. *Science* **1997**, *276*, 1425–1428.
- (25) Liu, C.; Li, M.; Dong, Z. X.; Jiang, D.; Li, X.; Lin, S.; Chen, D.; Zou, X.; Zhang, X. D.; Luker, G. D. Heterogeneous Micro-environmental Stiffness Regulates Pro-Metastatic Functions of Breast Cancer Cells. *Acta Biomater.* **2021**, *131*, 326–340.
- (26) Caliri, S. R.; Vega, S. L.; Kwon, M.; Soulas, E. M.; Burdick, J. A. Dimensionality and Spreading Influence Msc Yap/Taz Signaling in Hydrogel Environments. *Biomaterials* **2016**, *103*, 314–323.
- (27) Lou, J.; Stowers, R.; Nam, S.; Xia, Y.; Chaudhuri, O. Stress Relaxing Hyaluronic Acid-Collagen Hydrogels Promote Cell Spreading, Fiber Remodeling, and Focal Adhesion Formation in 3d Cell Culture. *Biomaterials* **2018**, *154*, 213–222.
- (28) Ekerdt, B. L.; Fuentes, C. M.; Lei, Y.; Adil, M. M.; Ramasubramanian, A.; Segalman, R. A.; Schaffer, D. V. Thermoreversible Hyaluronic Acid-Pnippam Hydrogel Systems for 3d Stem Cell Culture. *Adv. Healthcare Mater.* **2018**, *7*, No. 1800225.
- (29) Qu, T.; Jing, J.; Ren, Y.; Ma, C.; Feng, J. Q.; Yu, Q.; Liu, X. Complete Pulpodentin Complex Regeneration by Modulating the Stiffness of Biomimetic Matrix. *Acta Biomater.* **2015**, *16*, 60–70.
- (30) Cao, H.; Duan, L.; Zhang, Y.; Cao, J.; Zhang, K. Current Hydrogel Advances in Physicochemical and Biological Response-Driven Biomedical Application Diversity. *Signal Transduction Targeted Ther.* **2021**, *6*, No. 426.
- (31) Ozcan, B.; Bayrak, E.; Erisken, C. Characterization of Human Dental Pulp Tissue under Oscillatory Shear and Compression. *J. Biomech. Eng.* **2016**, *138*, No. 061006.
- (32) Shi, X.; Mao, J.; Liu, Y. Pulp Stem Cells Derived from Human Permanent and Deciduous Teeth: Biological Characteristics and Therapeutic Applications. *Stem Cells Transl. Med.* **2020**, *9*, 445–464.
- (33) Huang, Q.; Zou, Y.; Arno, M. C.; Chen, S.; Wang, T.; Gao, J.; Dove, A. P.; Du, J. Hydrogel Scaffolds for Differentiation of Adipose-Derived Stem Cells. *Chem. Soc. Rev.* **2017**, *46*, 6255–6275.
- (34) Silva, C. R.; Babo, P. S.; Gulino, M.; Costa, L.; Oliveira, J. M.; Silva-Correia, J.; Domingues, R. M. A.; Reis, R. L.; Gomes, M. E. Injectable and Tunable Hyaluronic Acid Hydrogels Releasing Chemotactic and Angiogenic Growth Factors for Endodontic Regeneration. *Acta Biomater.* **2018**, *77*, 155–171.
- (35) Liu, M. M.; Li, W. T.; Xia, X. M.; Wang, F.; MacDougall, M.; Chen, S. Dentine Sialophosphoprotein Signal in Dentineogenesis and Dentine Regeneration. *Eur. Cell Mater.* **2021**, *42*, 43–62.
- (36) Alqahtani, Q.; Zaky, S. H.; Patil, A.; Beniash, E.; Ray, H.; Sfeir, C. Decellularized Swine Dental Pulp Tissue for Regenerative Root Canal Therapy. *J. Dent. Res.* **2018**, *97*, 1460–1467.
- (37) Dewey, C. F., Jr; Bussolari, S. R.; Gimbrone, M. A., Jr; Davies, P. F. The Dynamic Response of Vascular Endothelial Cells to Fluid Shear Stress. *J. Biomech. Eng.* **1981**, *103*, 177–185.
- (38) Liang, C.; Liao, L.; Tian, W. Stem Cell-Based Dental Pulp Regeneration: Insights from Signaling Pathways. *Stem Cell Rev. Rep.* **2021**, *17*, 1251–1263.
- (39) Wang, X.; Li, F.; Xie, L.; Crane, J.; Zhen, G.; Mishina, Y.; Deng, R.; Gao, B.; Chen, H.; Liu, S.; Yang, P.; Gao, M.; Tu, M.; Wang, Y.;

Wan, M.; Fan, C.; Cao, X. Inhibition of Overactive Tgf-B Attenuates Progression of Heterotopic Ossification in Mice. *Nat. Commun.* **2018**, *9*, No. 551.

(40) Hwang, Y. C.; Hwang, I. N.; Oh, W. M.; Park, J. C.; Lee, D. S.; Son, H. H. Influence of Tgf- $\beta$ 1 on the Expression of Bsp, Dsp, Tgf- $\beta$ 1 Receptor I and Smad Proteins During Reparative Dentinogenesis. *J. Mol. Histol.* **2008**, *39*, 153–160.

(41) Lichtman, M. K.; Otero-Vinas, M.; Falanga, V. Transforming Growth Factor Beta (Tgf-B) Isoforms in Wound Healing and Fibrosis. *Wound Repair Regen.* **2016**, *24*, 215–222.

(42) Kim, K. K.; Sheppard, D.; Chapman, H. A. Tgf-B1 Signaling and Tissue Fibrosis. *Cold Spring Harbor Perspect. Biol.* **2018**, *10*, No. a022293.

(43) Margadant, C.; Sonnenberg, A. Integrin-Tgf-Beta Crosstalk in Fibrosis, Cancer and Wound Healing. *EMBO Rep.* **2010**, *11*, 97–105.

(44) Speight, P.; Kofler, M.; Szász, K.; Kapus, A. Context-Dependent Switch in Chemo/Mechanotransduction Via Multilevel Crosstalk among Cytoskeleton-Regulated Mrtf and Taz and Tgf- $\beta$ -Regulated Smad3. *Nat. Commun.* **2016**, *7*, No. 11642.

(45) Munger, J. S.; Huang, X.; Kawakatsu, H.; Griffiths, M. J.; Dalton, S. L.; Wu, J.; Pittet, J. F.; Kaminski, N.; Garat, C.; Matthay, M. A.; Rifkin, D. B.; Sheppard, D. The Integrin Alpha V Beta 6 Binds and Activates Latent Tgf Beta 1: A Mechanism for Regulating Pulmonary Inflammation and Fibrosis. *Cell* **1999**, *96*, 319–328.

(46) Maruri, D. P.; Iyer, K. S.; Schmidtke, D. W.; Petroll, W. M.; Varner, V. D. Signaling Downstream of Focal Adhesions Regulates Stiffness-Dependent Differences in the Tgf- $\beta$ 1-Mediated Myofibroblast Differentiation of Corneal Keratocytes. *Front Cell Dev. Biol.* **2022**, *10*, No. 886759.

(47) Szeto, S. G.; Narimatsu, M.; Lu, M.; He, X.; Sidiqi, A. M.; Tolosa, M. F.; Chan, L.; De Freitas, K.; Bialik, J. F.; Majumder, S.; Boo, S.; Hinz, B.; Dan, Q.; Advani, A.; John, R.; Wrana, J. L.; Kapus, A.; Yuen, D. A. Yap/Taz Are Mechanoregulators of Tgf-B-Smad Signaling and Renal Fibrogenesis. *J. Am. Soc. Nephrol.* **2016**, *27*, 3117–3128.

(48) Hiepen, C.; Mendez, P. L.; Knaus, P. It Takes Two to Tango: Endothelial Tgf- $\beta$ /Bmp Signaling Crosstalk with Mechanobiology. *Cells* **2020**, *9*, 1965.

(49) Zhang, T.; Wen, F.; Wu, Y.; Goh, G. S.; Ge, Z.; Tan, L. P.; Hui, J. H.; Yang, Z. Cross-Talk between Tgf-Beta/Smad and Integrin Signaling Pathways in Regulating Hypertrophy of Mesenchymal Stem Cell Chondrogenesis under Deferral Dynamic Compression. *Biomaterials* **2015**, *38*, 72–85.

## Recommended by ACS

### Realizing Holistic Charging–Discharging for Dendrite-Free Lithium Metal Anodes via Constructing Three-Dimensional Li<sup>+</sup> Conductive Networks

Tianci Cao, Yuefei Zhang, *et al.*

JANUARY 27, 2023  
ACS APPLIED MATERIALS & INTERFACES

READ 

### Rodlike FeS/SnS@N-C Core–Shell Microparticles for Lithium-Ion Batteries

Hui Zheng, Yuan Sang, *et al.*

FEBRUARY 09, 2023  
LANGMUIR

READ 

### Facile Approach for Improving the Interfacial Adhesion of Nanofiber Air Electrodes of Reversible Solid Oxide Cells

Zhiyi Chen, Kongfa Chen, *et al.*

FEBRUARY 03, 2023  
ACS APPLIED MATERIALS & INTERFACES

READ 

### Fabrication and Separation of EGaIn Microparticles from Human Blood Based on Dielectrophoresis Force and a W-Type Electrode

Yanfang Guan, Guangyu Liu, *et al.*

FEBRUARY 15, 2023  
LANGMUIR

READ 

Get More Suggestions >